Maximum Principle and Gradient Estimates for Stationary Solutions of the Navier-Stokes Equations; a partly experimental investigation

Robert Finn[1], Abderrahim Ouazzi[2], and Stefan Turek[2]

Department of Mathematics, Stanford University, USA[1]
Institute for Applied Mathematics, TU Dortmund, Germany[2]

Dedicated to Giovanni Paolo Galdi

Summary. We calculate numerically the solutions of the stationary Navier-Stokes equations in two dimensions, for a square domain with particular choices of boundary data. The data are chosen to test whether bounded disturbances on the boundary can be expected to spread into the interior of the domain. The results indicate that such behavior indeed can occur, but suggest an estimate of general form for the magnitudes of the solution and of its derivatives, analogous to classical bounds for harmonic functions.

The qualitative behavior of the solutions we found displayed some striking and unexpected features. As a corollary of the study, we obtain two new examples of non-uniqueness for stationary solutions at large Reynolds numbers.

Key words: Navier-Stokes equations, Maximum Principle, Gradient Estimates

1 Introduction

Two cornerstones of the theory of the Laplace equation

$$\triangle u = 0 \tag{1}$$

are the *a priori* bound on the solution, and the *a priori* bound on the gradient ∇u; see, e.g., [3], Chapter VIII, Theorems X and XII. The former bound states that if $u(x)$ is a solution of (1) in a bounded domain Ω and continuous up to $\Gamma = \partial\Omega$, then

$$\sup_{\Omega} |u| \leq M \doteq \max_{\Gamma} |u| \tag{2}$$

The latter bound states that there exists a function $\mathcal{F}(d;M)$ such that if d is distance from $p \in \Omega$ to Γ then

$$|\nabla u(p)| < \mathcal{F}(d;M). \tag{3}$$

The linearized (Stokes) equations of hydrodynamics

$$\begin{aligned} \triangle \boldsymbol{w} &= \nabla p \\ \operatorname{div} \boldsymbol{w} &= 0 \end{aligned} \tag{4}$$

for slow stationary viscous fluid flow, with velocity field $\boldsymbol{w}$ and pressure p, bear a formal resemblance to (1); this was exploited in a beautiful way by Odqvist [5] who showed that much of the classical Fredholm theory for (1) can be extended to solutions of (4). As a consequence, Odqvist was led to a bound

$$|\nabla \boldsymbol{w}(p)| < \mathcal{F}_{\Omega}(d;M) \tag{5}$$

analogous to (3), although Odqvist imposed also smoothness requirements on Γ that are not needed for (3). The subscript Ω in (5) indicates an additional distinction that occurs, that was not explicitly observed in [5]: *the functional dependence of* $\mathcal{F}$ *on* d *and on* M *can vary greatly, depending on the particular domain.* That was exhibited in [2], as a property of an explicitly known family of Couette flows, considered in expanding domains.

Given a domain Ω, the results of Odqvist lead to construction of a "Green's tensor" for the system (4) in Ω, and then to an integral equation for solutions of the Navier-Stokes equations

$$\begin{aligned} \triangle \boldsymbol{w} - \mathrm{R}e\, \boldsymbol{w} \cdot \nabla \boldsymbol{w} &= \nabla p \\ \operatorname{div} \boldsymbol{w} &= 0 \end{aligned} \tag{6}$$

in Ω, with prescribed boundary data subject to an outflow condition on Γ. Leray [4] studied the integral equation, and by an ingenious reasoning obtained an *a priori* bound for the Dirichlet integral for any solution and in consequence a bound for the gradient analogous to that of Odqvist; however the bound depends additionally on the Reynolds number Re and on the tangential derivatives of the data on Γ up to third order; see, e.g., the comments in [1]. Using that bound in the integral equation, Leray was able to prove the existence of a smooth solution of (6), in any domain bounded by smooth components, corresponding to sufficiently smooth data having zero outflow on each boundary component. It is a remarkable result that had not been predicted and certainly was unexpected, in view of the known instabilities that arise with increasing Re.

The question, whether for a specific domain there is a gradient bound for (6) fully analogous to that of Odqvist (i.e., depending only on Re and on M and not on smoothness of the boundary data), remains open. Such a bound would remove the differentiability requirements imposed by Leray on the data, and would also be of independent interest, in many contexts. Partial information was supplied by Finn and Solonnikov [2], who obtained a result of somewhat different character, weakening the requirements imposed by Leray but not yet including the specific estimate that is sought. Those authors offered a suggestive reasoning (short of a proof) that in two dimensions the indicated estimate may fail.

In the present note, we put the matter to an initial experimental test in the two dimensional case, using numerical calculations. We take as domain Ω a square, and impose data on the sides Γ that are uniformly bounded but successively more oscillatory, to determine whether the rapid disturbances on the boundary will spread into the interior. We do that for two ranges of data that are tangential on Γ, so that no fluid enters Ω but for which the tangential direction oscillates. We do it also for two ranges of data that are orthogonal on Γ, with rapid oscillation between entering Ω and leaving it. Each calculation was performed for three different Reynolds numbers, in a range from 1 to $10,000$, and for five different oscillation rates, determined by a parameter k. We use the computer calculations to estimate the magnitudes $|\boldsymbol{w}|$ in Ω. The corresponding bounds on $|\nabla \boldsymbol{w}|$ are then inferred from Theorem 1 in [2].

2 Test configurations

Specifically, the data were as follows, for velocities $\boldsymbol{w} = (u, v)$ on the sides $x = \pm 1$, $y = \pm 1$ of a square of side length 2:

A) Tangential data

A1) $\boldsymbol{w} = ((x^2 - 1)\sin kx, 0)$ on $y = \pm 1$, $\boldsymbol{w} = (0, 0)$ on $x = \pm 1$

AC) $\boldsymbol{w} = ((x^2 - 1)\sin kx, 0)$ on $y = +1$, $\boldsymbol{w} = (0, (y^2 - 1)\sin ky)$ on $x = +1$ and
$\boldsymbol{w} = (0, 0)$ on the remaining sides

$$k = 1, \cdots, 120; \ \mathrm{R}e = 1, \cdots, 10,000.$$

B) Normal data

B1) $\boldsymbol{w} = (0, (x^2 - 1)\sin kx)$ on $y = \pm 1$, $\boldsymbol{w} = (0, 0)$ on $x = \pm 1$

BC) $\boldsymbol{w} = (0, (x^2 - 1)\sin kx)$ on $y = 1$, $\boldsymbol{w} = (-(y^2 - 1)\sin ky, 0)$ on $x = 1$ and
$\boldsymbol{w} = (0, 0)$ on the remaining sides

$$k = 1, \cdots, 120; \ \mathrm{R}e = 1, \cdots, 10,000.$$

We examined also the question, whether a local jump discontinuity in boundary data can spread into the interior as an unbounded disturbance. In the view that such behavior could be dependent on the magnitude of the jump, we made the choices:

C) Tangential data

$\boldsymbol{w} = (K, 0)$ on $y = \pm 1$, $-0.9 < x < +0.9$; $\boldsymbol{w} = (0, 0)$ elsewhere on the boundary

D) Normal data

$\boldsymbol{w} = (0, K)$ on $y = \pm 1$, $-0.9 < x < +0.9$; $\boldsymbol{w} = (0, 0)$ elsewhere on the boundary

$$K = 1, \cdots, 60; \; \mathrm{R}e = 1, \cdots, 10,000.$$

3 Numerical methods

In our numerical studies with the open source CFD package FeatFlow (`www.featflow.de`), we mainly focus on low order Stokes elements with nonconforming finite element approximations for the velocity and piecewise constant pressure functions which satisfy the LBB condition [7]. Moreover, in the case of nonstationary flow simulations, second order time stepping schemes are used which can be applied in a fully coupled as well as operator-splitting, resp., pressure correction framework. However, in these studies, we directly solved the stationary Navier-Stokes equations by applying a Newton-like method to the fully coupled discretized system while the auxiliary linear problems are solved via multigrid techniques.

There are well-known situations for standard FEM methods when severe numerical problems may arise, namely in the case of convection dominated problems. Then, numerical difficulties arise for instance for medium and high Re numbers since the standard Galerkin formulation usually fails and may lead to numerical oscillations and to convergence problems of the iterative solvers. Among the stabilization methods existing in the literature for these types of problems, we use the proposed one in [6, 8] which is based on the penalization of the gradient jumps over element boundaries. In 2D, the additional stabilization term $\mathbf{J}\boldsymbol{u}$, acting only on the velocity $\boldsymbol{u}$ in the momentum equations, takes the following form (with $h_E = |E|$)

$$\langle \mathbf{J}\boldsymbol{u}, \boldsymbol{v} \rangle = \sum_{\text{edge E}} \max(\gamma \frac{1}{\mathrm{R}e} h_E, \gamma^* h_E^2) \int_E [\nabla \boldsymbol{u}] : [\nabla \boldsymbol{v}] \, ds, \tag{7}$$

and can simply added to the original bilinear form. Summarizing, in the underlying test cases which require the solution of stationary problems, efficient

Newton-type and multigrid solvers can be easily applied for such highly accurate stabilization techniques (see [8] for more details) which are the basis of the subsequent numerical analysis.

4 Results and Analysis

In the data for cases **A** and **B**, the factors of the form $\left(x^2-1\right)$ are inserted to impose continuity with zero data at the corner points, thus ameliorating eventual singularities that could arise from the corner boundary discontinuities. Although the presence of these discontinuities causes both the domain and the data to be outside the range for Lerays existence theorem, the choice made was considered preferable from the point of view of programming data for the computer procedures. No indication was observed of any difficulty in finding at least one solution of the boundary problem in all cases, and in some instances multiple solutions could be identified, see the discussion below. The choice $k=120$, which appears only in Figures 1 and 3, was not originally contemplated; it is outside the range for which the computation procedures can be trusted to be reliable, and so the inferences we make from that case must be considered provisional; however the results obtained for it are consistent with other observations, and point to trends that we feel are worth noting.

An initial comment is in order on the choice of scaling for the figures, which display interior velocity magnitudes on a color scale ranging from blue (small) to red (large). One is tempted as a “natural” choice to make the highest scale point in each figure the maximum velocity magnitude in the figure. Such a procedure is well suited for examining what happens in that figure, but can be misleading when comparing one figure with another. In consideration of the behavior features that we felt most important to emphasize, and with a view to minimize confusion in interpretation, we decided to choose the highest scale point for each row to be the maximum of the two numbers: a) the maximum velocity magnitude achieved in that row, and b) the maximum velocity magnitude achieved in any row that is above that one. The reader should keep that choice in mind when interpreting the figures; a change in scale in any figure can produce a very different appearance of the figure. In the relevant (groups of) Figures 1 to 4, k increases with row from top to bottom, Re increases with column from left to right. Thus in our choice of scaling, the highest scale point is the same for all figures in a row, and is non-decreasing from top to bottom.

It should be noted that the maximum boundary velocity magnitude is the same for all figures in a row. For reference, the values for this quantity are: $k=1:.365; k=3:.784; k=15:.989; k=30:.997; k=60:.999; k=120:$ 1.000. For the data as chosen, this maximum magnitude is usually achieved at only a single point. In some of the figures, the highest scale points will be slightly less than these values; that is because the computer mesh points in general differ from those special extremal points.

We organize our interpretations of the figures according to Roman numerals.

I. Figure 1 displays the velocity magnitudes $|\boldsymbol{w}|$ in case A1 corresponding to five values of k and three values of Re, arising from oscillating tangential data on the sides $y = \pm 1$ for which no fluid enters or leaves the square Ω. The value $k = 15$ is not included in the figure, however the $k = 15$ fluid patterns are similar to those for $k = 1$ and $k = 3$ cases. The maximum magnitudes interior to Ω for some of the cases are roughly comparable to those on Γ, and in that sense one sees that the boundary disturbances do transmit into the interior.

   With increasing k and small Re, the oscillations in data are dissipated rapidly by frictional forces within the fluid; there appears to be no focusing of energy, and to the extent visible in the figures, one can not even discern that the boundary data are achieved, although the oscillations in data are detectable near the boundary. We have suppressed the case R$e = 100$ in the interest of more clarity for the remaining cases, but we remark that the behavior does not differ greatly from that of R$e = 1$.

   For large Re this behavior changes dramatically, and a ring of relatively large kinetic energy appears with increasing k when Re is large enough. For fixed Re and further increasing k, the effect fades and for R$e \leq 1000$ disappears. Presumably it will eventually disappear also for larger Re, as suggested in the figure. Thus, for large Re a rotational symmetry not apparently connected with the boundary data at first occurs with increasing k, but as k increases further the effect then is overwhelmed by dissipation and washes out. It should be noted that throughout this development, the magnitudes interior to Ω do not exceed the maximum on the boundary.

   We examine the effect in further detail in Figures 7 and 8, which offer relief figures for the magnitudes, with the particular choices $k = 3$ and $k = 30$, with increasing Re. The "spikes" on opposite sides are the prescribed boundary data.

   The flow within the rings is roughly rotational, and can be produced in either rotation sense, depending on details of the computational procedure. Thus *we obtain a new example of non-uniqueness for stationary solutions of (6) at large Reynolds number*. The two solutions are illustrated in Figure 9, for $k = 30$ and for R$e = 1000$ and $10,000$.

II. In order to determine the extent to which the symmetry of the data affected the results, the same oscillating data were imposed on two adjacent sides. Results are shown in Figure 2, The same qualitative behavior occurs, with somewhat larger magnitudes appearing, presumably since the boundary data are imposed on sides that are closer together.

III. Figure 3 results from identical data normal to the boundary, imposed on the top and bottom of the square, with $k = 1, 3, 30, 60, 120$, and $\mathrm{R}e = 1, 1000, 10,000$. A notable event occurs when k changes from 1 to 3, with $\mathrm{R}e = 10,000$. Presumably due to more rapidly changing data and larger magnitudes, the entering flow for $k = 3$ does not succeed in crossing to the opposite side as does the flow for $k = 1$, but instead enters and then leaves again on the same side. It is for this reason that we decided to retain the case $k = 1$ for display, despite that no full oscillation occurs. It exhibits an initial step in a behavior that seems to exert a controlling influence on the further developments.

The change to $k = 30$ in that column is again dramatic, with the development of a circular flow as in the tangential data case. What appears to be happening is that flow enters the square and then departs in adjacent boundary segments. For large k these segments are close together and most of that motion occurs close to the boundary, as indicated by the succession of half-rings in the figure. Space then appears in the central part of the square for development of the observed large circular motion, with larger velocities than occur near the boundary. The magnitudes in the central ring become for normal data notably larger than occurs for tangential data. There is clear evidence of energy focusing, with magnitudes in the ring more than double those of the (isolated) boundary peaks.

For each k the top and bottom boundary segments are divided into an even number $2j = 2(1 + [k/\pi])$ of subsegments, in each of which flow either enters or exits, and such that for each subsegment on either half of the boundary in which flow is entering, there is a corresponding one on the other half in which flow is leaving. Flow alternately enters and leaves in adjacent subsegments. If j is odd, then a predominantly left oriented flow near the upper boundary will be created, as will a predominantly right oriented flow near the lower boundary, see Figure 10a. The reverse orientation occurs when j is even, see Figure 10b. The flows thus occasioned provide an explanation for the development of the circular flow in the central region.

The determination of orientation just described is reasonable when k is not large. As k increases, the subsegments near the vertices lose their influence in view of the factor $(x^2 - 1)$, and the actual flow could be established in either direction, determined by circumstances having nothing to do with the equations. That could be an explanation for non-uniqueness of computed solutions. In fact, in Figure 3 with $Re = 10,000$ the computed flow orientation reverses from $k = 30$ to 60, although j is even in both cases, and again from 60 to 120, when j reverses parity.

We note however that the non-uniqueness we have already observed under I above occurred for tangential data, for which a corresponding reasoning does not at first seem available to us. In that case the data and also the figures seem to suggest a succession of symmetrically placed small eddies at the boundary in alternating orientations; these lead formally to symmetric influence on a symmetrically placed interior circle, which would not induce rotation.

In fact, we believe the interior rotation arises in the tangential data case from quite different causes, than for the normal data case.

The clue to what happens for tangential data can be found in the upper two rows of Figure 1. The behavior in the $\mathrm{R}e = 10,000$ column of those rows is sketched in Figure 11a, where flow directions are shown. One sees there that a large-scale rotational motion in the interior of the square is indeed supported by the data, and occurs as the result of an instability of the symmetric solution. This can happen in either rotation sense, as indicated in Figure 11b, and as can be seen by comparing the second and third columns for the upper two rows of Figure 3. With increasing k, the effects become more complicated, and combine to lead at large k and $\mathrm{R}e$ to a nearly circular configuration.

Thus, we must expect in this situation the existence of at least three distinct solutions: a solution exhibiting the symmetries of the symmetric data but which is unstable to skew-symmetric rotational disturbances, and then two rotational solutions with opposite flow orientations, as there is no reason to prefer one orientation to the other. It is these two rotational solutions that give rise to the non-uniqueness observed in item I above.

IV. Again for normal data we reduced the symmetry by placing the data on adjacent sides instead of opposite sides. Again the same kind of behavior appeared, with larger interior magnitudes presumably occasioned by the sides being closer together.

V. We consider Figures 5 and 6, arising from successively increasing constant data on fixed subsegments of opposite boundary segments, with a jump to zero data at the endpoints. Here the behavior yielded clearly less dramatic events. Interior magnitudes in some instances exceeded those of the boundary data, but not by large amounts. This is noteworthy, especially as the boundary data are identically their maxima on intervals close to the entire sides in length, rather than at a few isolated points as in the earlier cases. On comparing behavior in the two situations, it becomes clear that rapid boundary oscillations do propagate into the interior and cause disturbances that can be large in relation to the boundary magnitudes.

5 Some conclusions

We may interpret the figures from the point of view of the a priori estimates discussed in the Introduction. Looking at Figures 2, 4, 5 and 6 we see immediately that *the estimate* $|\boldsymbol{w}| < M$ *does not extend without change from solutions of (1) to solutions of (6)*; larger values can be attained throughout large interior sets, including even the midpoint of the square. However, from Figures 5 and 6 we see no evidence that even a large jump discontinuity in data will induce arbitrarily large magnitudes in the interior. The calculations suggest that with increasing k, oscillating disturbances may initially spread into the interior and even exhibit some focusing behavior, but as k becomes large enough, the focusing dampens out due to frictional dissipation. Thus, we are inclined to expect an *a priori* estimate of the form $|\boldsymbol{w}| < \mathcal{F}_\Omega(Re; M)$. From Theorem 1 of [2] would then follow an estimate $|\nabla \boldsymbol{w}| < \mathcal{G}_\Omega(d; Re; M)$.

We emphasize again that although our calculations suggest such estimates, we have not proved them.

Acknowledgement. We are indebted to John Heywood for helpful comments. This work was supported by the German Research Association (DFG) through the collaborative research center SFB/TRR 30 and through the grants TU 102/21-1. The initial author thanks the Max-Planck-Institut für Mathematik in den Naturwissenschaften, in Leipzig, for its hospitality during preparation of the work.

References

[1] Finn, R. On the Steady-State Solutions of the Navier-Stokes equations, III. *Acta Mathematica*, 105:197–244, 1961.

[2] Finn, R. and Solonnikov, V. A. Gradient estimates for solutions of the Navier-Stokes equations. *Top. Meth. Nonl. Anal.*, 9:29–39, 1997.

[3] Kellogg, O. D. *Foundations of Potential Theory.* Ungar Publishing Co., 1929. New York.

[4] Leray, J. Étude de diverses équations intégrales non linéaires et de quelquess problèmes que pose l'hydrodynamique. *J. Math. Pures Appl.*, 12:329–375, 1933.

[5] Odqvist, F. K. G. Über die Randwertaufgaben der Hydrodynamik zäher Flüssigkeiten. *Math. Z.*, 32:1–82, 1930.

[6] Ouazzi, A. *Finite Element Simulation of Nonlinear Fluids. Application to Granular Material and Powder.* Shaker Verlag, Achen, 2006. ISBN 3-8322-5201-0.

[7] Rannacher, R. and Turek, S. A simple nonconforming quadrilateral Stokes element. *Numerical Methods for Partial Differential Equations*, 8:97–112, 1992.

[8] Turek, S. and Ouazzi, A. Unified edge–oriented stabilization of nonconforming FEM for incompressible flow problems: Numerical investigations. *J. Numer. Math.*, 15:299–322, 2007.

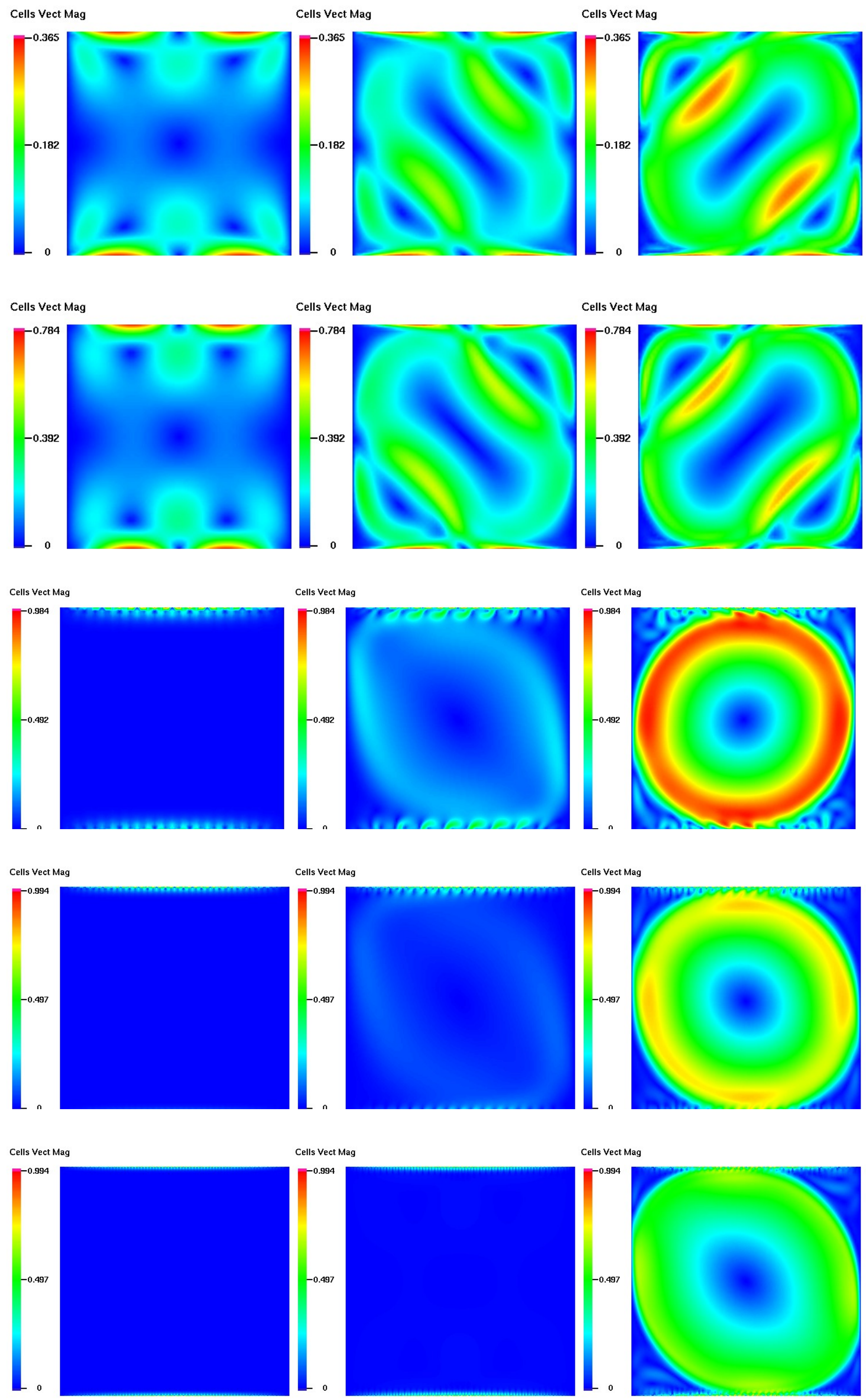

Fig. 1. *The tangential data A1: Velocity magnitude for $k = 1$, $k = 3$, $k = 30$, $k = 60$ and $k = 120$ and Reynolds numbers $Re = 1$, $Re = 1,000$ and $Re = 10,000$. Reynolds number increases from left to right and k increases from top to bottom*

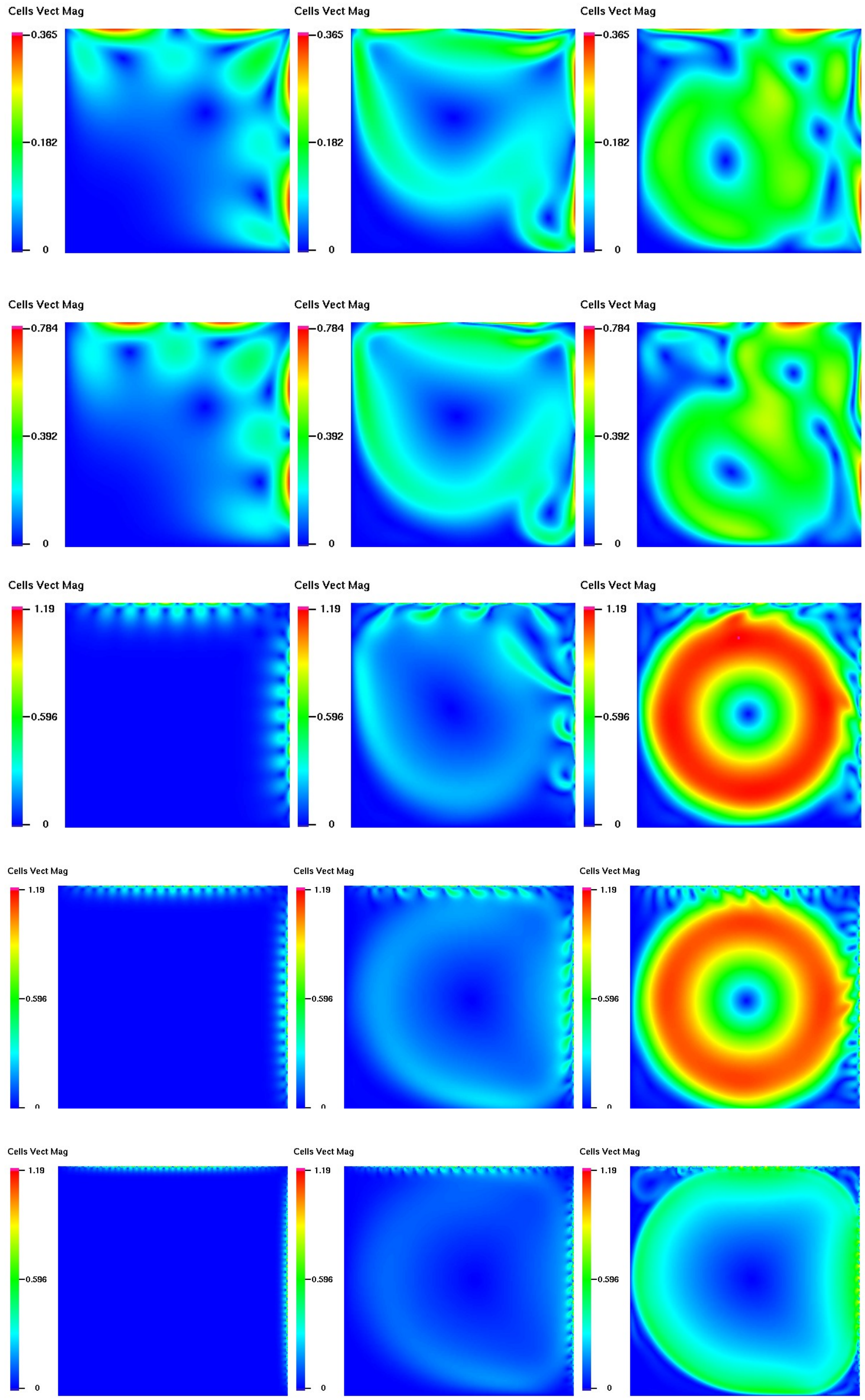

Fig. 2. *The tangential data AC: Velocity magnitude for $k = 1$, $k = 3$, $k = 15$, $k = 30$ and $k = 60$ and Reynolds numbers $Re = 1$, $Re = 1,000$ and $Re = 10,000$. Reynolds number increases from left to right and k increases from top to bottom*

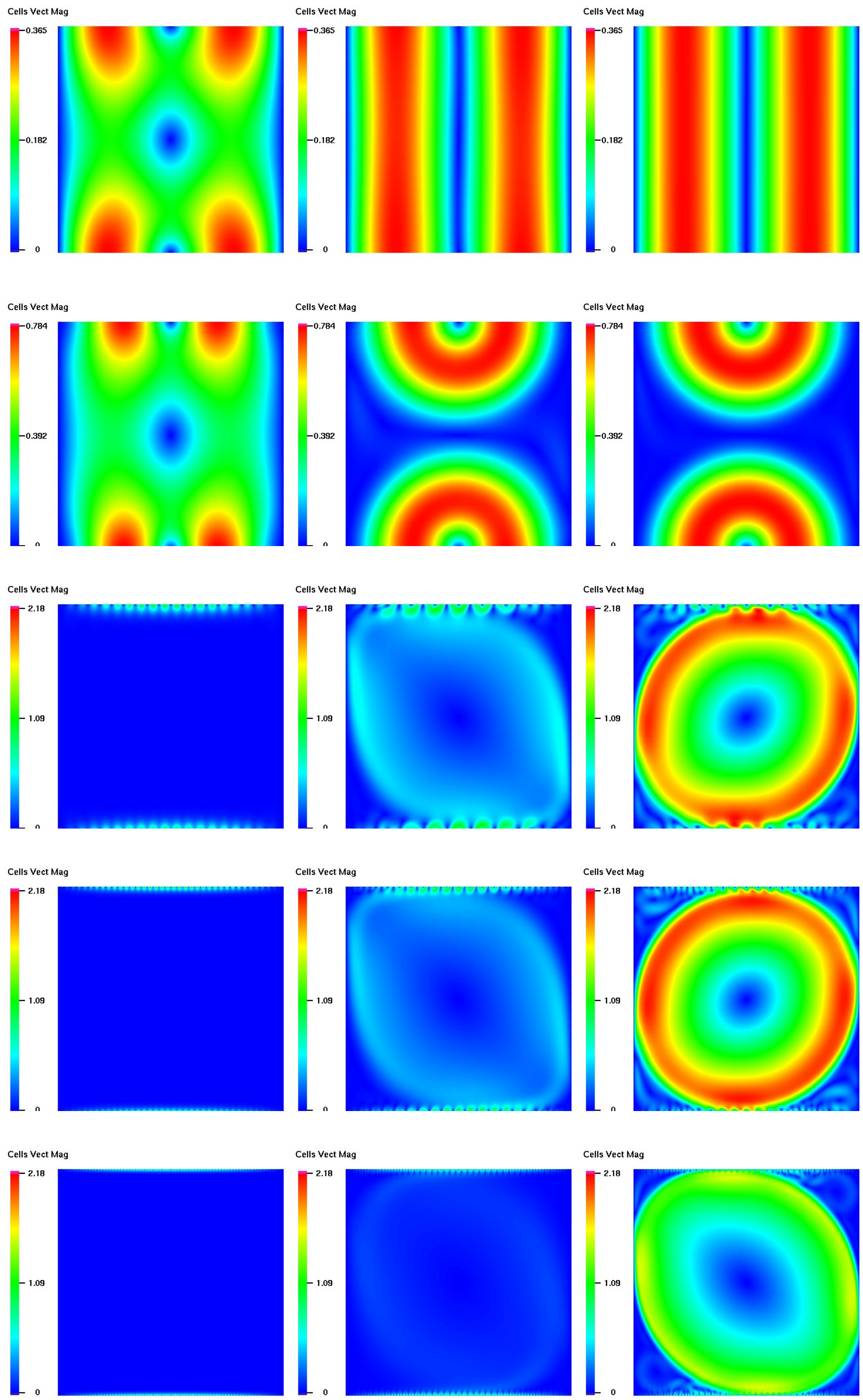

Fig. 3. *The normal data B1: Velocity magnitude for* $k = 1$, $k = 3$, $k = 30$, $k = 60$ *and* $k = 120$ *and Reynolds numbers* $Re = 1$, $Re = 1,000$ *and* $Re = 10,000$. *Reynolds number increases from left to right and* k *increases from top to bottom*

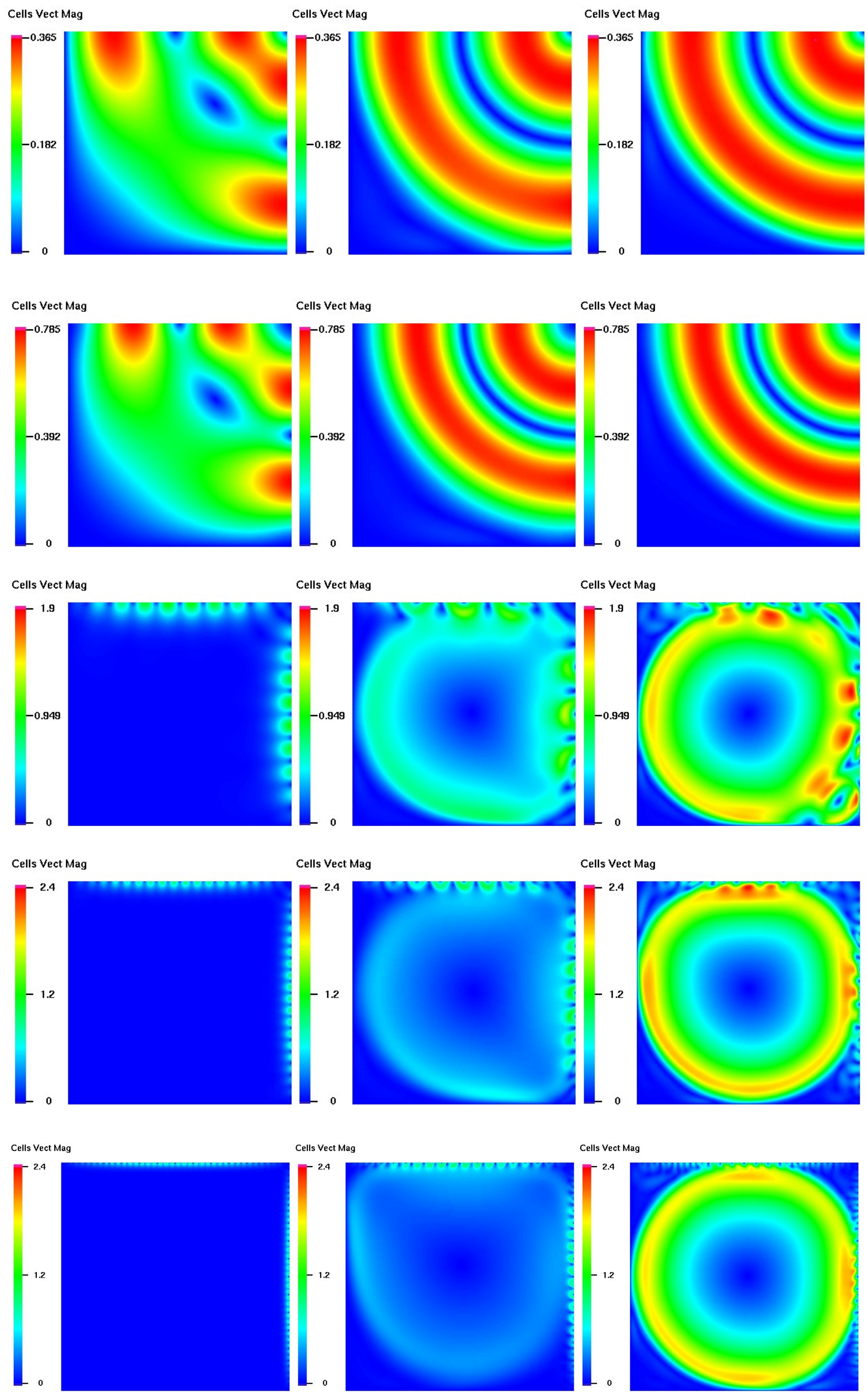

Fig. 4. *The normal data BC: Velocity magnitude for $k = 1$, $k = 3$, $k = 15$, $k = 30$ and $k = 60$ and Reynolds numbers $Re = 1$, $Re = 1,000$ and $Re = 10,000$. Reynolds number increases from left to right and k increases from top to bottom*

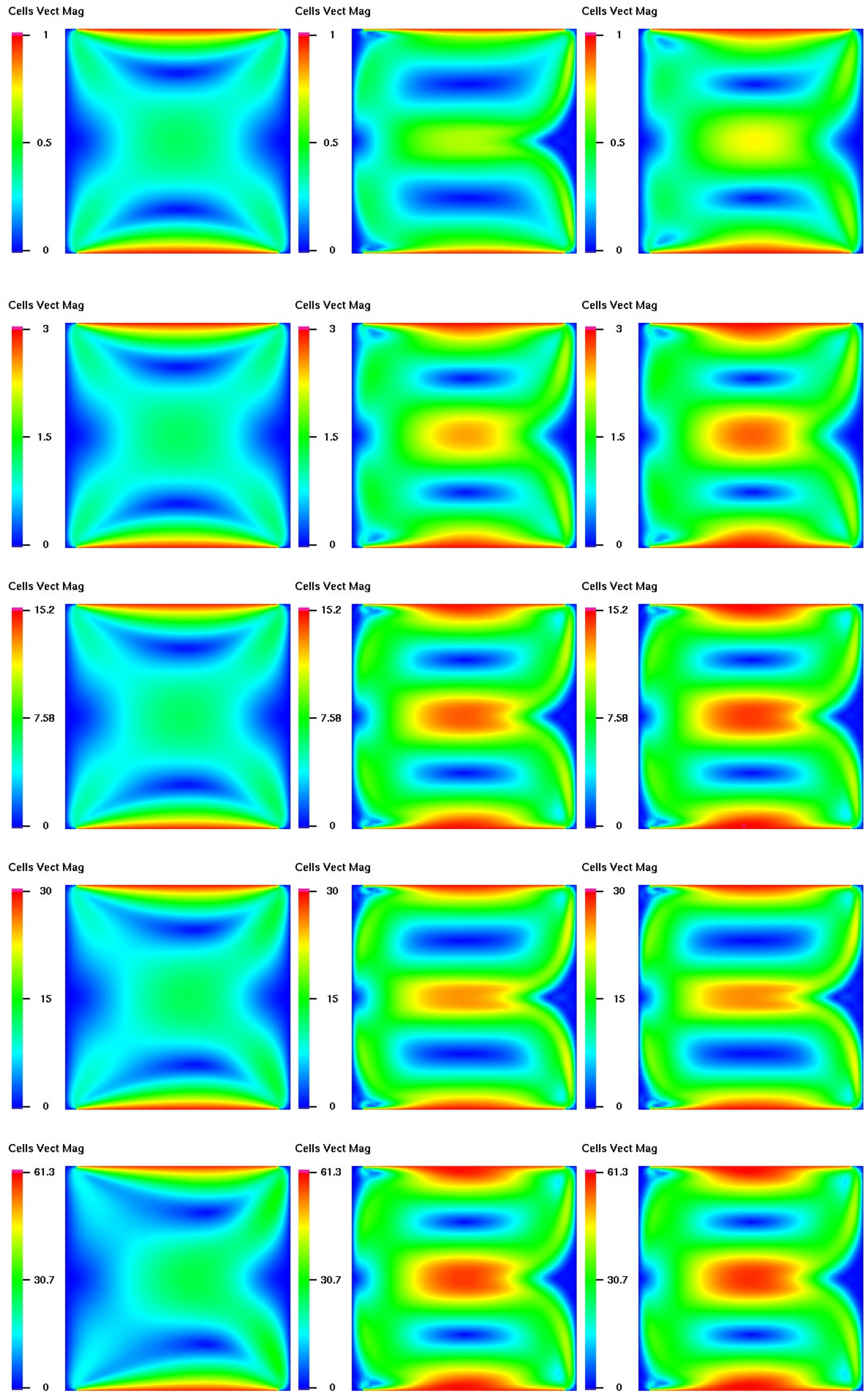

Fig. 5. *The tangential data C*: Velocity magnitude for $K = 1$, $K = 3$, $K = 15$, $K = 30$ and $K = 60$ and Reynolds numbers $Re = 1$, $Re = 1,000$ and $Re = 10,000$. Reynolds number increases from left to right and K increases from top to bottom

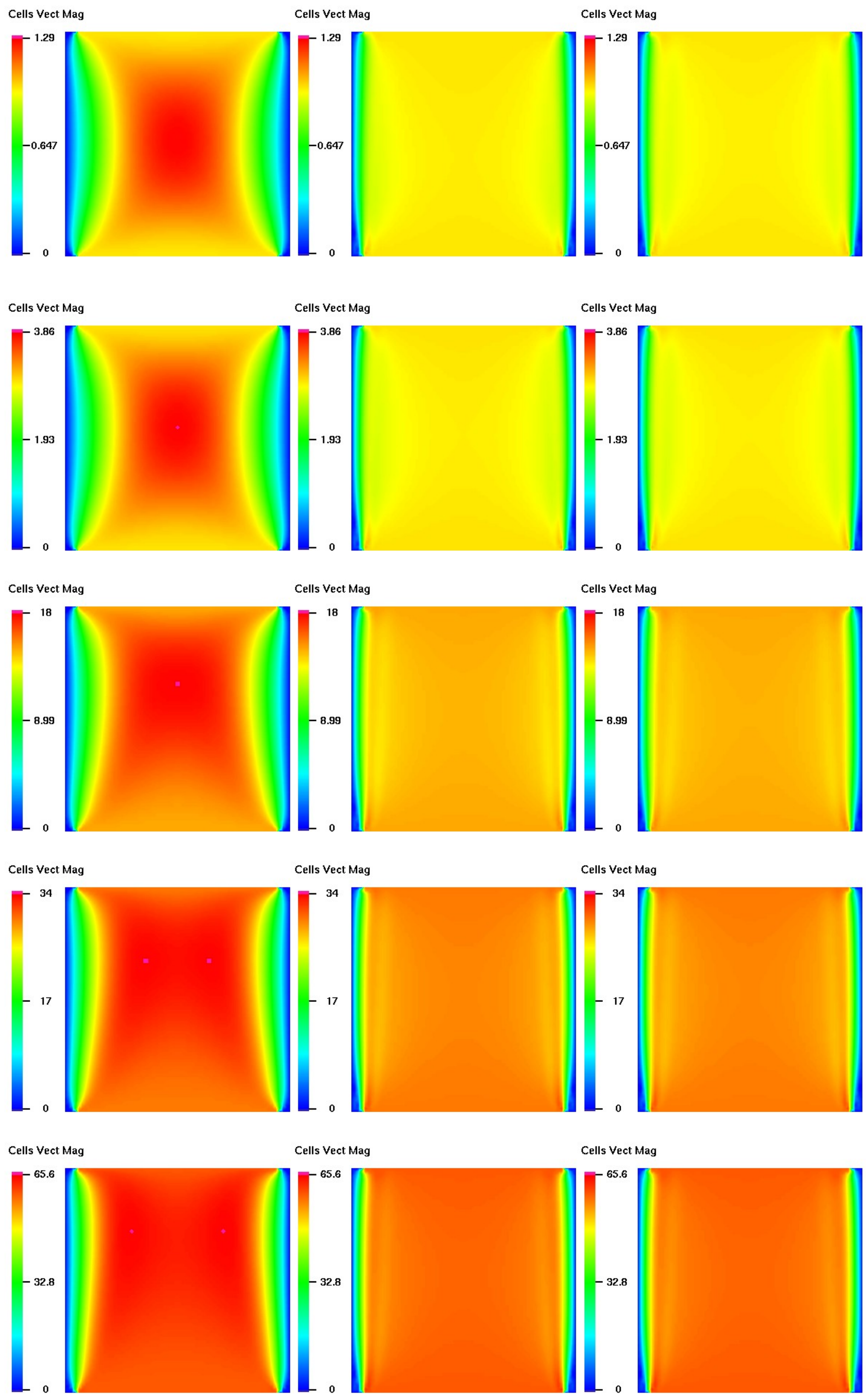

Fig. 6. *The normal data D*: Velocity magnitude for $K = 1$, $K = 3$, $K = 15$, $K = 30$ and $K = 60$ and Reynolds numbers $Re = 1$, $Re = 1,000$ and $Re = 10,000$. Reynolds number increases from left to right and K increases from top to bottom

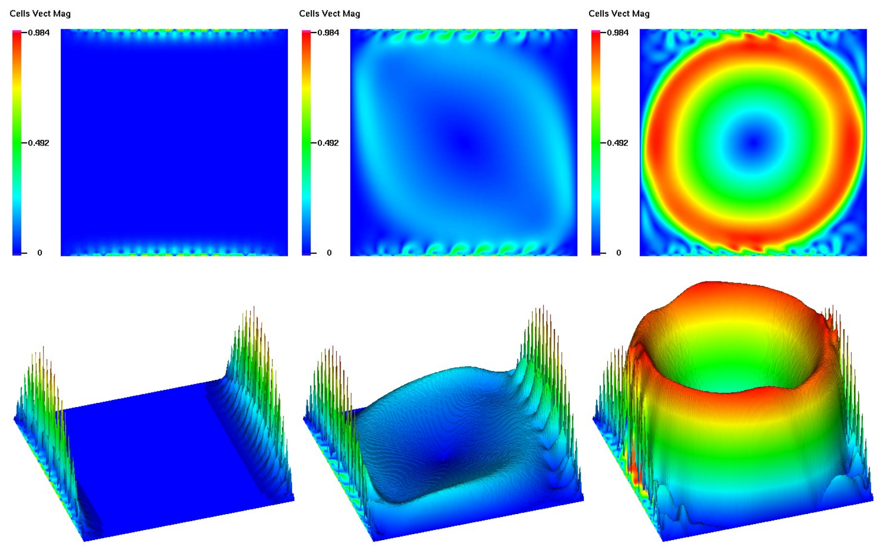

Fig. 7. *The tangential data A1*: Solution (top) and corresponding three dimensional view of the solution (bottom) for $k = 30$ and $Re = 1$, $Re = 1,000$ and $Re = 10,000$. Reynolds number increases from left to right

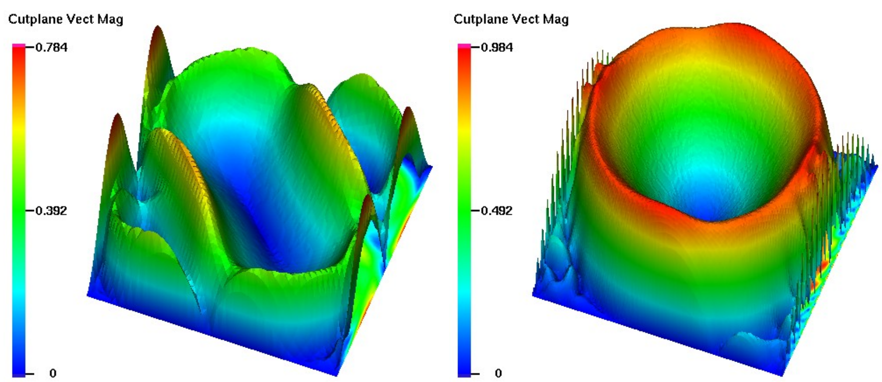

Fig. 8. *The tangential data A1*: A three dimension of the norm of the velocity for $k = 3$ and $k = 30$ for $Re = 10,000$

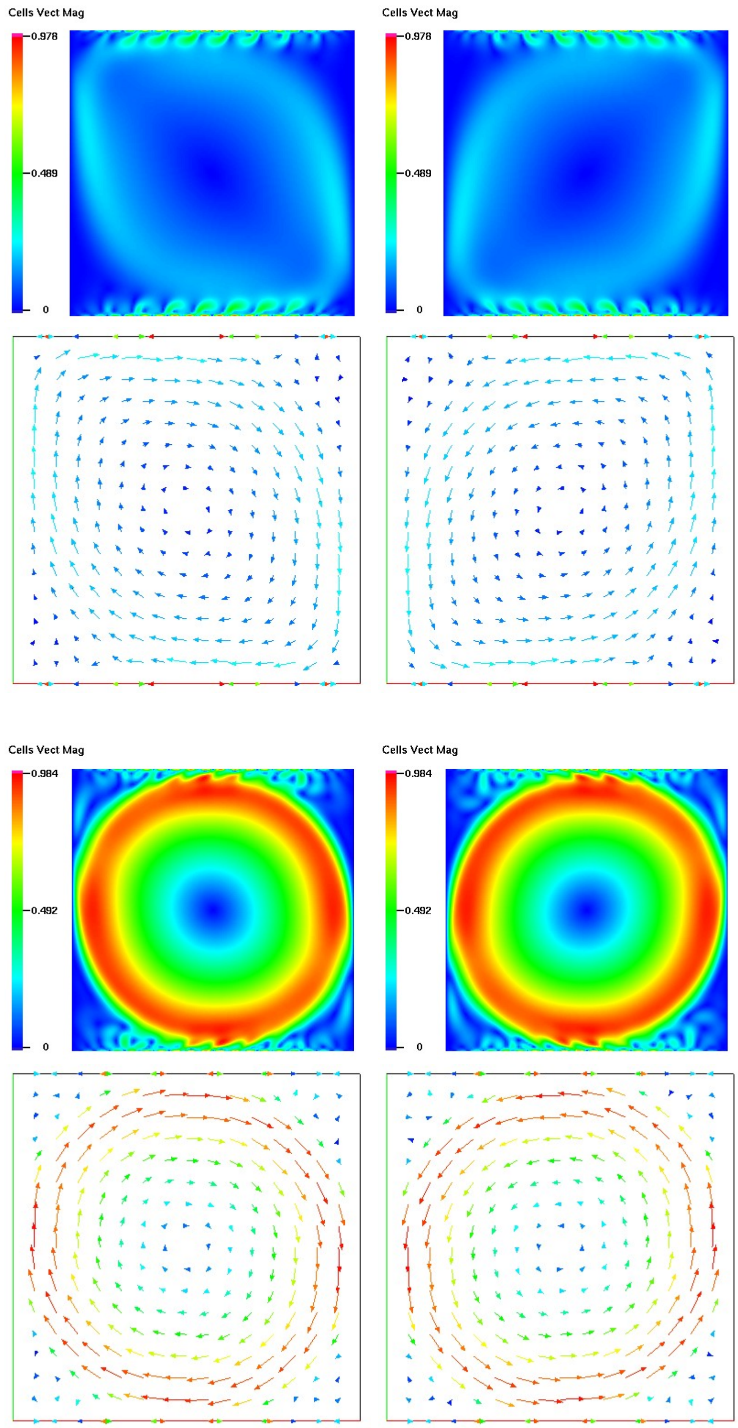

Fig. 9. *The tangential data A1*: Solution and the corresponding vector plot for $k = 30$ and $Re = 1,000$, and $Re = 10,000$, arising from changes in detail of the calculation procedure for case A (Fig. 1). Reynolds number increases from top to bottom.

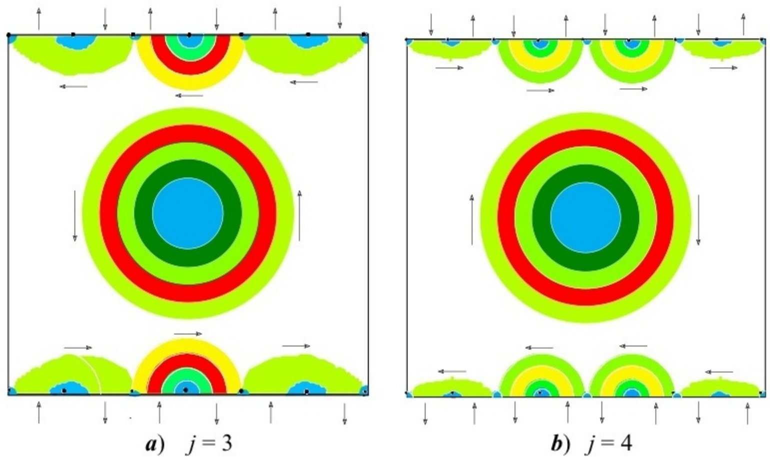

Fig. 10. *The normal data B1*: Projected explanation for development of rotation interior to the square, in Case B1. The arrows exterior to the square indicate the directions of applied data in the intervals separated by dots on the sides. Fluid enters between two dots and exits in an adjacent interval. Identical data are prescribed on the top and bottom of the square. The boundary motions combine to induce rotation in the center. Note that orientation reverses from j = 3 to j = 4. These numbers were chosen for illustration; they may be too small for actual development of interior rotation.

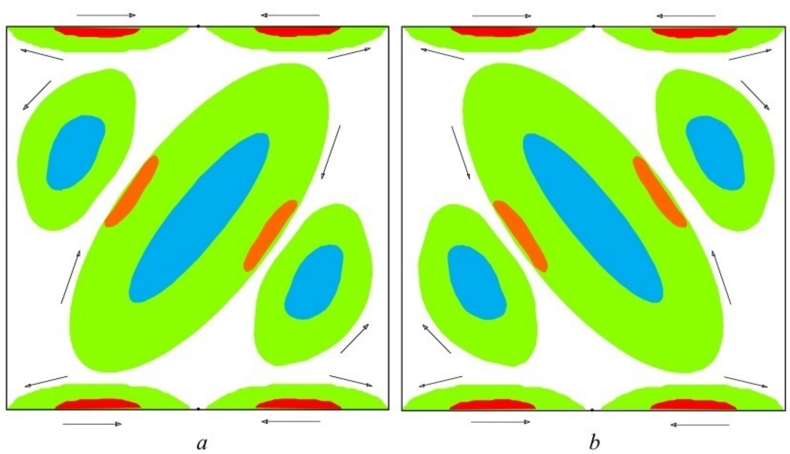

Fig. 11. *The tangential data A1*: Development of large-scale interior rotation in case k = 1 or 3, as result of instability of symmetric flow. Two distinct configurations with opposite flow orientations appear, in addition to a presumed symmetric solution.